Research Square

Preprints are preliminary reports that have not undergone peer review.
They should not be considered conclusive, used to inform clinical practice,
or referenced by the media as validated information.

Deep Feature Selection and Multi-Sparsity Functional Connectivity Networks for Autism Classification

Lei Zhang

chray@cqjtu.edu.cn

Chongqing Jiaotong University

Yupan Ding

Wuhan University

Zhanpeng Zheng

Chongqing Jiaotong University

Hong Zhu

Chongqing Jiaotong University

Lei Huang

Chongqing Jiaotong University

Research Article

Keywords:

Posted Date: November 4th, 2026

DOI: https://doi.org/10.21203/rs.3.rs-11239833/v1

License: This work is licensed under a Creative Commons Attribution 4.0 International License.
Read Full License

Additional Declarations: No competing interests reported.

Deep Feature Selection and Multi-Sparsity Functional Connectivity Networks for Autism Classification

Lei Zhang[1,*], Yupan Ding[2], Zhanpeng Zheng[1], Hong Zhu[1], Lei Huang[1]

[1]School of Mathematics and Statistics, Chongqing Jiaotong University, Chongqing 400074, China

[2]School of Artificial Intelligence, Wuhan University, Wuhan, China

[*]Corresponding author: chray@cqjtu.edu.cn

Abstract

Autism spectrum disorder (ASD) is associated with heterogeneous alterations in functional brain organization, making reliable neuroimaging-based characterization difficult. We developed a framework combining deep feature selection with multi-sparsity functional connectivity networks to identify discriminative connectivity patterns and classify ASD. Resting-state functional magnetic resonance imaging data from 871 participants in the Autism Brain Imaging Data Exchange I dataset (403 ASD and 468 typically developing controls) were analyzed. Pearson correlation networks were constructed across 111 regions and thresholded at multiple sparsity levels. Deep feature selection identified stable connections across training folds, while nested cross-validation selected the optimal sparsity level and evaluated a linear support vector machine. The framework achieved 86.2% accuracy, 88.8% sensitivity, 84.0% specificity, and an area under the curve of 91.6%. Discriminative connections were concentrated in frontal, occipital, and parietal regions, including the superior frontal gyrus and lateral occipital cortex. These findings show that combining feature selection with multi-sparsity connectome analysis can improve the identification of reproducible autism-associated connectivity patterns. The results should be interpreted as research-level classification rather than a clinical diagnostic test and require independent external validation.

Keywords: autism spectrum disorder, resting-state functional MRI, functional connectivity, deep feature selection, brain network sparsity

1 Introduction

Autism spectrum disorder (ASD) is a complex and heterogeneous neurodevelopmental condition characterized by challenges in social interaction, communication, and the presence of repetitive, restrictive behaviors and interests. The exact etiology of ASD remains inadequately understood, and it is often comorbid with neurodevelopmental disorders [1, 2]. Due to the disorder's complexity and variability, early diagnosis and intervention are essential not only to facilitate timely support but also to improve long-term functional outcomes for affected individuals. However, current diagnostic practices primarily depend on behavioral assessments and clinical observations, with a notable absence of reliable and consistent biomarkers [3, 4].

Functional magnetic resonance imaging (fMRI) has been widely employed to examine brain functional connectivity in ASD [5]. By measuring variations in blood oxygenation, fMRI allows non-invasive investigation of neural activity and inter-regional connectivity [6-9]. Large-scale initiatives such as the Autism Brain Imaging Data Exchange (ABIDE) have aggregated extensive fMRI datasets from multiple laboratories worldwide, providing critical resources for studying ASD while introducing significant analytical challenges.

Research has revealed widespread disruptions in functional connectivity across several brain networks in individuals with ASD. Altered intrinsic connectivity within the default mode network (DMN) has been linked to specific ASD symptoms [10]. Structural and functional abnormalities at key DMN nodes, as well as atypical connections between these nodes and other regions, appear to contribute to the manifestation of ASD traits [11]. Furthermore, impairments in executive function may arise from reduced adaptability and integrative capacity of frontoparietal-insular control regions within the functional network [12]. Chen et al. proposed that disruptions in multisensory brain circuitry might be essential for the early development of behavioral skills and the emergence of autism symptomatology in young children with ASD [13]. Other region-of-interest (ROI)-based studies have identified aberrant connectivity in the Superior Frontal Gyrus and Lateral Occipital Cortex as potentially relevant to social cognition and visuospatial processing deficits in ASD [14, 15], providing biologically interpretable targets for further investigation. These findings suggest that neural underpinnings of ASD are intricately linked to aberrant functional connectivity within specific brain networks.

In recent years, researchers have increasingly explored the application of machine learning and deep learning techniques for the classification and prediction of ASD. Deep learning, especially convolutional neural networks (CNNs) and graph convolutional networks (GCNs), has shown significant advantages in processing high-dimensional and complex data [14, 15]. For example, Hu et al. developed an interpretable segmented fully connected neural network,

achieving high accuracy rates [16]. Rakhimberdina et al. constructed a population graph using various combinations of imaging and phenotypic features, integrating multiple graph-based models with neural network architectures, which resulted in a 73.1% accuracy on the ABIDE dataset [17]. Shao et al. introduced a heterogeneous graph convolutional attention network model that combines attention mechanisms with heterogeneous GCNs, achieving an 82.9% accuracy in classifying the ABIDE dataset [18]. Although these approaches are powerful, they often face two limitations: (1) a lack of explicit interpretability regarding the contribution of specific functional connections or ROIs, and (2) insufficient consideration of network sparsity, which can be critical in small-sample, high-dimensional neuroimaging scenarios.

However, existing methods have not yet fully leveraged functional connectivity features to elucidate the neural mechanisms of ASD. Li et al. introduced a deep feature selection model that identifies informative features with nonlinear behavior by selecting them at the input layer of deep neural network [19]. Shao et al. applied this approach to the ABIDE dataset, extracting functional connectivity features from fMRI data and achieving a 79.5% accuracy by constructing a graph convolutional network (GCN) for classification [20]. Chen et al. proposed a comprehensive framework for high-dimensional nonlinear variable selection using deep neural networks within a supervised learning context. This method utilizes a deep neural network comprising selection and approximation layers to model nonlinear systems. Its sparsity and feature selection capabilities enable it to identify the most significant variables within high-dimensional feature spaces, thereby improving its adaptability to medical classification tasks [21].

Deep learning-based classification methods and feature extraction techniques are often designed for scenarios with very large sample sizes and relatively few features. However, medical datasets frequently face the challenge of small sample sizes, complicating the direct application of these methods to the "small n, large p" problem [22]. To address this issue, we propose a support vector machine (SVM) classification method that integrates deep feature selection (DFS) with multi-sparsity functional connectivity networks. Specifically, we begin by constructing functional connectivity networks based on the correlations between different brain regions of the subjects. We then apply a connectivity retention strategy with varying thresholds to induce different levels of sparsity in these networks. Next, we use the DFS method to filter out functional connections that are highly associated with autism [21]. To further refine feature selection, we employ an inner cross-validation strategy to determine the optimal sparsity level for the functional connectivity networks, based on different degrees of network sparsity. Finally, we classify the data using the features from the optimally sparse brain networks. We tested this method on the ABIDE dataset, demonstrating its effectiveness in handling the small sample size and high dimensionality characteristic of medical datasets.

The main contributions of this approach are as follows:

1. The proposed method leverages functional brain networks with varying levels of sparsity and integrates DFS to extract critical functional connections related to ASD.

2. The proposed method achieved an accuracy of 86.2% and an AUC of 91.6% on ABIDE I and showed higher performance than the selected comparison methods under the reported evaluation protocol.

3. Our method revealed critical brain region connections, particularly in the Superior Frontal Gyrus and Lateral Occipital Cortex, that exhibit strong discriminative power across different sparsity levels, providing insights into the neural mechanisms underlying ASD.

The remainder of this article is organized according to the IMRaD structure. The Methods section describes the ABIDE I cohort, preprocessing, multi-sparsity network construction, deep feature selection, and nested cross-validation. The Results section reports classification performance and the identified connectivity patterns. The Discussion interprets the findings, considers limitations, and summarizes the conclusions.

2 Methods

2.1 Data Acquisition and Preprocessing

The proposed framework was evaluated using the ABIDE I dataset, a widely used multisite resource in autism research. This multi-site dataset collects resting-state fMRI scans together with corresponding phenotypic information from 17 research institutions worldwide. In total, ABIDE I contains imaging data from 1112 participants, including 539 subjects diagnosed with ASD and 573 typically developing (TD) individuals. For consistency with widely adopted experimental protocols, we followed the data inclusion strategy reported in Abraham and Parisot [23, 24]. As a result, a subset of 871 participants with reliable data quality was retained for subsequent analysis. This curated cohort consists of 403 ASD subjects and 468 TD controls. A detailed summary of the selected subjects is provided in Table 1.

ABIDE provides data processed through multiple standardized pipelines for connectome construction, including the Connectome Computation System, the Configurable Pipeline for the Analysis of Connectomes (CPAC), and the Data Processing Assistant for Resting-State fMRI [25-27]. In our study, we followed the preprocessing protocol used by Parisot et al., opting for the CPAC pipeline due to its configurability. These pipelines incorporate a comprehensive

Table 1: Demographic Descriptive Statistics of the 871 Subjects Selected from the ABIDE Dataset.

Site	ASD			TD		
	Age	Sex (M/F)	FIQ	Age	Sex (M/F)	FIQ
CALTECH	24.0±7.6	4/1	99.5±2.6	28.2±12.2	6/4	111.0±9.2
CMU	26.0±5.4	4/2	109.5±12.1	27.8±4.4	3/2	116.4±10.2
KKI	10.7±1.3	9/3	97.7±20.6	10.1±1.2	15/6	112.3±9.8
LEUVEN	18.2±5.1	23/3	109.4±13.1	18.4±4.9	26/4	115.4±13.1
MAX MUN	28.4±13.2	16/3	108.5±15.0	25.2±8.4	26/1	111.7±9.5
NYU	14.8±7.1	64/10	107.4±16.4	15.8±6.2	72/26	113.4±13.1
OHSU	11.4±2.2	12/0	106.0±22.0	10.2±1.0	13/0	114.1±11.1
OLIN	17.1±3.3	11/3	110.2±20.1	16.9±3.6	12/2	116.4±13.9
PITT	18.3±7.0	21/3	111.1±14.8	18.7±6.7	22/4	109.5±8.9
SBL	34.0±6.6	12/0	106.5±14.1	33.6±6.8	14/0	N/A
SDSU	15.3±1.8	8/0	123.1±11.6	14.0±1.9	13/6	107.3±10.5
STANFORD	10.2±1.6	9/3	115.1±15.6	9.8±1.7	9/4	112.9±15.2
TRINITY	17.0±3.2	19/0	108.2±16.5	17.1±3.8	25/0	110.9±12.2
UCLA	13.2±2.5	42/6	101.0±12.7	13.0±2.0	32/5	107.4±9.9
UM	13.7±2.4	38/9	109.3±16.4	14.8±3.6	55/18	108.4±9.8
USM	23.6±8.4	43/0	99.6±17.0	20.9±8.3	24/0	115.5±15.4
YALE	13.1±3.0	14/8	94.2±22.8	13.6±2.1	11/8	103.2±15.9
Total	17.1±8.0	349/54	105.8±17.1	16.8±7.2	378/90	111.1±12.1

FIQ: Full-Scale Intelligence Quotient. Age and FIQ are reported as mean ± standard deviation. FIQ information is missing for TD participants from the SBL site.

set of preprocessing procedures, such as removal of non-brain tissue, correction for slice acquisition timing and head motion, normalization of global signal intensity, elimination of nuisance-related confounds, and temporal band-pass filtering in the frequency range of 0.01–0.1 Hz. In addition, all functional images were spatially normalized to a common anatomical reference space.

Concerning the regions of interest (ROIs) in the brain, we adopt the Harvard-Oxford (HO) atlas as the reference. This atlas, which comes with the FSL software suite, comprises both cortical and subcortical probabilistic atlases, enabling the division of the entire brain into 111 distinct ROIs. These regions include critical structures such as the Thalamus, Caudate, and Putamen [28-31], providing a comprehensive framework for neuro-imaging analysis. For each subject, the functional connectivity brain network was quantified by computing the Pearson correlation coefficients. Let $\mathbf{X} = \{\mathbf{X}^1, \mathbf{X}^2, \cdots, \mathbf{X}^{871}\}$ denote the raw data for all the subjects. For each $\mathbf{X}^k$, a corresponding $\mathbf{W}^k$ is generated, where $\mathbf{W}^k \in \mathbb{R}^{111\times111}$ is a symmetric matrix with each element representing the correlation between the i-th and j-th brain regions.

2.2 Brain Networks with Different Sparsity Levels

The functional connectivity network constructed with Pearson correlation coefficients captures all the pairwise associations between brain regions, leading to a densely connected network. This may include blood-oxygen-level-dependent (BOLD) noise. To refine the network and reduce noise, we applied a thresholding process. By setting thresholds at different percentiles

of $\mathbf{W}$, we retained the functional connections whose absolute values exceeded thresholds, thereby generating brain networks with varying degrees of sparsity. We constructed multiple sparse brain networks using thresholds at the following percentiles: 0, 5, 10, 15, 20, 25, 30, 35, 40, 45, and 50. A threshold of 0 corresponds to the 0-th percentile of the weight matrix, meaning that all the correlation connections are retained. Conversely, a threshold of 50 corresponds to the 50-th percentile, indicating that only the top 50% of the strongest correlations are retained. This thresholding strategy is used to mitigate noise effects and to create sparse correlation matrices [32]. This process is expressed as follows:

$$W_{ij}^{(new)} = \begin{cases} W_{ij}, & |W_{ij}| > \text{threshold} \\ 0, & otherwise \end{cases} \tag{1}$$

where W_{ij} denotes the i-th row and the j-th column element in matrix $\mathbf{W}^k$.

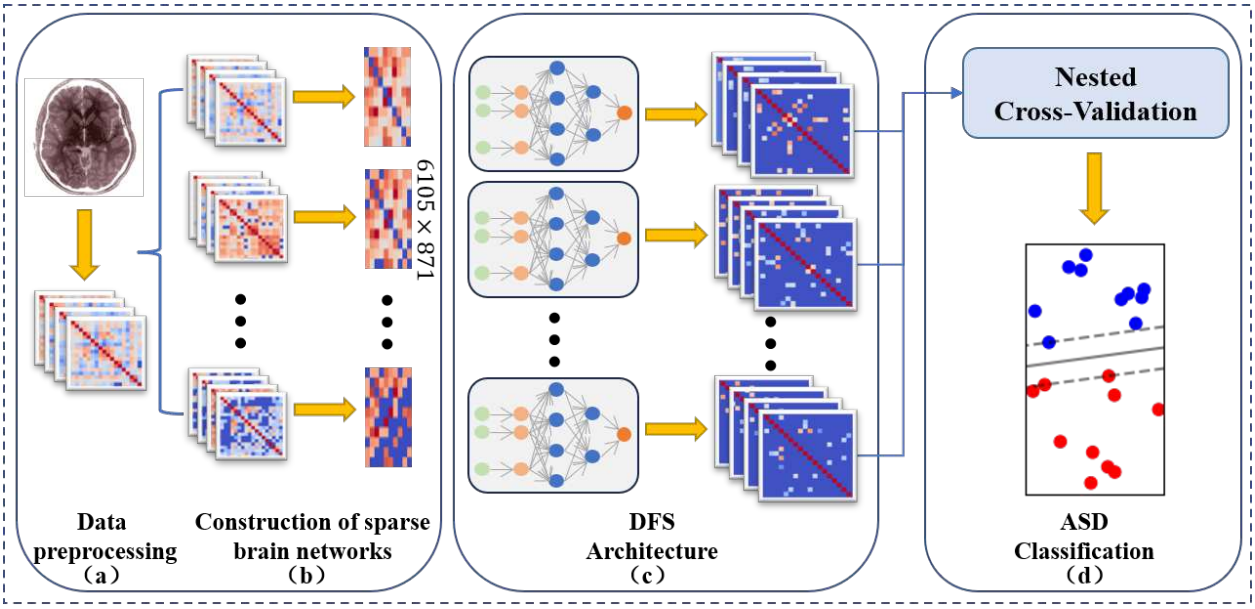


Fig. 1: Flowchart of DFS and multi-sparsity functional connectivity networks for enhanced ASD classification. (a) Data preprocessing and construction of correlation-based brain networks. (b) Construction of brain networks with varying sparsity levels and dimensionality reduction to 6105 dimensions, where 871 represents the number of subjects. (c) Neural network-based DFS frameworks are used to extract key functional connections. (d) Nested cross-validation is employed to select the optimal sparsity level for the brain networks, which are used for SVM classification.

2.3 Deep Feature Selection and Classifier Learning

Medical datasets face the challenge of having a small sample size but a large feature dimensionality, referred to as the "small n, large p" problem. After obtaining the sparsified correlation

matrix $\mathbf{W}^{k(new)}$ from (1), we first extract only its upper triangular part while removing the diagonal self-connections [33, 34]. This step reduces redundancy and computational cost, but does not change the total number of unique connectivity features derived from the matrix. For our data, each functional connectivity matrix contains $N(N-1)/2 = 6105$ unique connections, where N is the number of brain regions. Flattening the upper triangular part into a row vector yields

$$\mathbf{w}^k = \text{vec}(\text{triu}\mathbf{W}^{k(new)}), \tag{2}$$

where $\mathbf{w}^k$ is the functional connectivity vector of length 6105 for the k-th subject, triu$(\cdot)$ denotes the operation of extracting the upper triangular part of the matrix, and vec$(\cdot)$ refers to the operation of flattening the matrix row-wise into a vector. At this stage, we obtain a feature matrix of size 871×6105 (samples $\times$ features).

Even after extracting only the upper triangular part of the above functional connectivity matrix, we still retain a feature set of 6105 dimensions for 871 samples. We employed the DFS method proposed by Chen et al. [21], which uses deep neural networks composed of selection and approximation layers. This DFS method is designed for high-dimensional nonlinear variable selection within a supervised learning framework. The core idea behind DFS is to convert the feature selection problem into a sparse constraint optimization problem. In this approach, sparse parameters are used in the selection layer to identify the most relevant features, while other parameters are employed in the approximation layer to model the relationships between the selected features and the target variables. This dual-layer design allows for efficient feature selection, improving the model's performance and interpretability. With DFS, we reduce the dimensionality of the feature set and retain the most informative features, thereby enhancing the predictive power and generalization performance of our models.

$$\begin{aligned} \min_{\mathbf{w},\Theta} \quad & \frac{1}{n}\sum_{k=1}^{n} \ell\left(y_k h(\mathbf{w}^k; \mathbf{w}, \Theta)\right) + \lambda_1 \|\mathbf{w}\|_F^2 \\ & + \lambda_2 \|\Theta\|_2^2, s.t., \ \|\mathbf{w}\|_0 \leq s, \end{aligned} \tag{3}$$

where ℓ is the cross-entropy loss function, y_k is the true label of the k-th sample, $h(\cdot)$ is the fitting function of the neural network, $\mathbf{w}^k$ is the functional connectivity vector of length 6105 for the k-th subject, obtained from (2), $\mathbf{w}$ is the final sparse weight vector of length 6105, initially randomly generated, and Θ represents the other parameters in the approximation layer. $\|\cdot\|_F$ denotes the Frobenius norm, s is a positive integer controlling the sparsity, and λ_1 and λ_2 are the regularization parameters.

We performed five-fold cross-validation to identify important features from the dataset.

Given the inherent variability in dataset splitting and the differences across multi-site data, the feature distributions generated in each fold of the training set may vary. To ensure that the features selected by the above DFS method exhibit robust adaptability, we applied a stringent feature retention criterion: a feature is retained in the final subset only if it appears consistently across all the folds. Features that do not meet this criterion are discarded. This process can be formally described as follows:

$$w_f = \begin{cases} \frac{1}{m} \sum_{i=1}^{m} |w_{f,i}|, if\ f\ \in \mathcal{F}_i\ for\ all\ i \\ 0,\ otherwise \end{cases}, \tag{4}$$

where w_f is the final weight assigned to feature f. The weight is computed as the average of the absolute values of the feature's weights across all m folds, if the feature f appears in every fold's feature subset $\mathcal{F}_i$. Specifically, $w_{f,i}$ is the weight of feature f in the i-th fold, obtained from $\mathbf{w}$ in (3). If feature f is not present in all the folds, its weight w_f is set to 0. The term m denotes the total number of folds in the cross-validation.

After identifying the important feature subset, we employed ten-fold nested cross-validation to select the most appropriate sparse network for each subset. Specifically, the data set was divided into training and testing sets according to the ten-fold cross-validation scheme. Each training set was further split into inner training and inner testing sets. Within the inner training sets, we trained models using feature subsets with varying levels of sparsity, selecting the subset that performed best on the inner testing sets. This optimal subset was then evaluated on the outer testing sets. The process was repeated for all the folds, and the final performance was obtained by averaging the results across the ten outer testing sets. For classification, we used a support vector machine (SVM) with a linear kernel. According to statistical learning theory, more complex models typically require larger sample sizes [35]. Using a more complex classifier may lead to over-fitting. The overall workflow is illustrated in Fig. 1.

3 Results

3.1 ASD Classification Performance

We have investigated the impact of different feature selection methods on performances of classifier. These methods included Principal Component Analysis (PCA), Autoencoders (AE), Multi-Layer Perceptron (MLP), and DFS. For PCA, we extracted features corresponding to [10, 30, 50, 80, 100, 200, 300, 400, 500, 600, 700, 800, 850, 871], ranging from the top 10

principal components to all the components. When using all the components, it indicates that they could explain 100% of the variance. For the other three methods, we extracted features with the following numbers: [50, 80, 500, 1000, 1500, 2000, 2500, 3000, 3500, 4000, 4500, 5000, 5500, 6000]. It is noteworthy that we tested using all the 6,105 features, corresponding to the original functional connectivity input. For a fair comparison, we fixed the learning rate at 0.005 for the three neural network-based methods (AE, MLP, and DFS). Both AE and MLP used a batch size of 32 and 50 epochs.

The DFS module serves as the core feature selection component in our framework. In our implementation, DFS consists of two fully connected hidden layers: the first hidden layer contains 50 neurons, and the second hidden layer contains 10 neurons. Both layers employ the ReLU activation function. The output layer is a softmax layer with two output neurons corresponding to the binary classification task. Network weights are initialized using the default initialization strategy, and biases are initialized to zero.

A sparse selection layer is applied prior to the hidden layers, controlled by a target sparsity parameter $s = 1000$, which specifies the maximum number of features to retain in each iteration. The sparsity constraint is progressively enforced using a step size of 5 and a temperature parameter of 25 to smooth the feature selection probabilities.

Two separate Adam optimizers are used: one for the selection layer with a weight decay coefficient of 0.0005, and another for the entire network with a weight decay coefficient of 0.0025. The learning rate for both optimizers is set to 0.005. The cross-entropy loss function is used as the optimization objective.

The model is trained for 10 epochs, with the feature support set updated at each epoch. During training, the model exhibiting the minimum validation loss is selected as the best-performing model, and the corresponding feature subset is recorded as the final selected feature set. Unless otherwise specified, the above parameter settings are used as the default configuration for all experiments. These hyperparameters were empirically chosen to balance convergence stability, selection sparsity, and classification performance.

Table 2 shows the performance of each feature selection method as the number of features varies. We report multiple evaluation metrics, including Accuracy (ACC), Sensitivity (SEN), Specificity (SPE), AUC, F1 Score and Precision. Sensitivity is particularly crucial in disease diagnosis, as it reflects the true positive rate, which indicates the ability of a screening test to correctly identify patients with the condition. From Table 2, one can observe that the DFS method achieves a significantly higher classification accuracy, outperforming conventional feature selection approaches. Among the other three methods, PCA exhibits the best performance, while AE and MLP methods yield relatively poorer results. Additionally, we compared our method with state-of-the-art methods, including DFC+SVM [36],

Table 2: Performance Comparisons of Different Feature Selection Methods.

Method	Features	ACC (%)	SEN (%)	SPE (%)	AUC (%)	F1 (%)	Precision (%)
PCA	300	73.0±3.4	67.0±11.3	78.2±10.2	74.4±5.5	69.3±5.7	73.8±6.7
AE	1000	69.4±6.3	65.6±16.2	72.9±17.3	70.6±7.1	65.8±8.4	70.6±11.5
MLP	1000	69.6±3.2	68.3±9.8	70.7±10.2	70.2±5.4	67.3±4.3	67.5±4.9
DFS	1000	**86.2±2.4**	**88.8±4.5**	**84.0±6.9**	**91.6±1.7**	**85.7±2.0**	**83.3±6.0**

All results are averaged from ten-fold cross-validation.

Table 3: Comparison of Methods on the ABIDE Dataset (871 Subjects)

Method	Atlas	ACC (%)	AUC (%)
DFC+SVM [36]	AAL	76.8	81.0
MVS+GCN [37]	AAL	69.8	69.0
AE+DNN [38]	Power	79.2	82.4
WL-DeepGCN [39]	HO	77.3	82.6
HCAN [18]	HO	82.1	84.6
DFS+SVM [Ours]	HO	**86.2**	**91.6**

MVS+GCN [37], AE+DNN [38], WL-DeepGCN [39], and HCAN [18], in Table 3. These methods utilized the ABIDE dataset and selected the same cohort of 871 participants (403 ASD and 468 TD). Our method achieved the highest results in both ACC and AUC, showing higher ACC and AUC than the selected comparison methods under the reported evaluation protocol. For context, the comparison methods are summarized below:

- **DFC+SVM**: Time series are extracted from predefined brain regions based on the Automated Anatomical Labeling (AAL) atlas. Dynamic functional connectivity (DFC) is constructed by dividing the time series into non-overlapping windows and computing Pearson correlation coefficients between regions within each window. A multi-task feature selection scheme that combines elastic net and manifold regularization is applied to identify discriminative features. Classification is finally performed using a multi-kernel SVM, where Gaussian kernels corresponding to different feature subsets are integrated for prediction.

- **MVS+GCN**: A multi-view graph convolutional network is proposed to jointly learn graph structures and multi-task embeddings, aiming to mitigate noise and heterogeneity in brain networks. The model captures shared patterns across sparse networks constructed at different thresholds through a common embedding space, while enforc-

ing view consistency. In addition, prior subnetwork regularization is incorporated to emphasize biologically relevant systems, such as the salience and default mode networks.

- **AE+DNN**: A deep learning framework is developed for ASD classification based on functional brain networks from resting-state fMRI. Networks are constructed using Pearson correlations among 264 ROIs defined by the Power atlas, from which topological features are extracted and normalized. An autoencoder (AE) is employed to learn compact latent representations, and its encoder is combined with additional layers to perform binary classification.

- **WL-DeepGCN**: The framework integrates functional connectivity networks and population graphs using advanced graph neural networks. Edge weights are adaptively learned in a latent space by incorporating non-imaging attributes such as site, gender, and age. Recursive feature elimination is applied for dimensionality reduction, while random edge removal, dropout, and batch normalization are used to improve generalization and training stability.

- **HCAN**: A Heterogeneous Graph Convolutional Attention Network is proposed for ASD classification by jointly modeling fMRI and phenotypic data. A population graph is decomposed into multiple meta-path-based homogeneous graphs, each processed by residual GCNs, while a semantic attention mechanism weights their contributions. The fused representations are passed through dropout and an MLP classifier optimized with cross-entropy loss.

3.2 Comparison Across Feature Counts

We further investigated the performance of each method as the number of retained features varied, as shown in Fig. 2. It is clear that both the AE and MLP methods consistently yield suboptimal results, regardless of the number of features retained. This may be attributed to their inability to effectively capture important functional relationships across varying levels of sparsity. PCA demonstrated optimal performance with 300 features, beyond which incremental improvements were minimal. Conversely, the DFS method maintained an accuracy above 80% when limited to 3000 features or fewer. However, its accuracy experienced a significant drop as the number of features increased. This decline can likely be attributed to the inclusion of non-informative features, which, beyond a certain threshold, can hinder the classification process.

It is noted that while 3000 features were initially considered, the final feature set used for classification was significantly reduced. This reduction was achieved by retaining only

the most critical features that consistently emerged across all folds of cross-validation. For example, in a dense functional brain network with 1000 features, we extracted and ranked the weights of each functional connection. As depicted in Fig. 3, each of the five folds of cross-validation retained 1000 important features, effectively eliminating 5105 functional connections from the original 6105. However, the final ranking of functional connections identified only 530 as the most significant, representing the shared features across all folds.

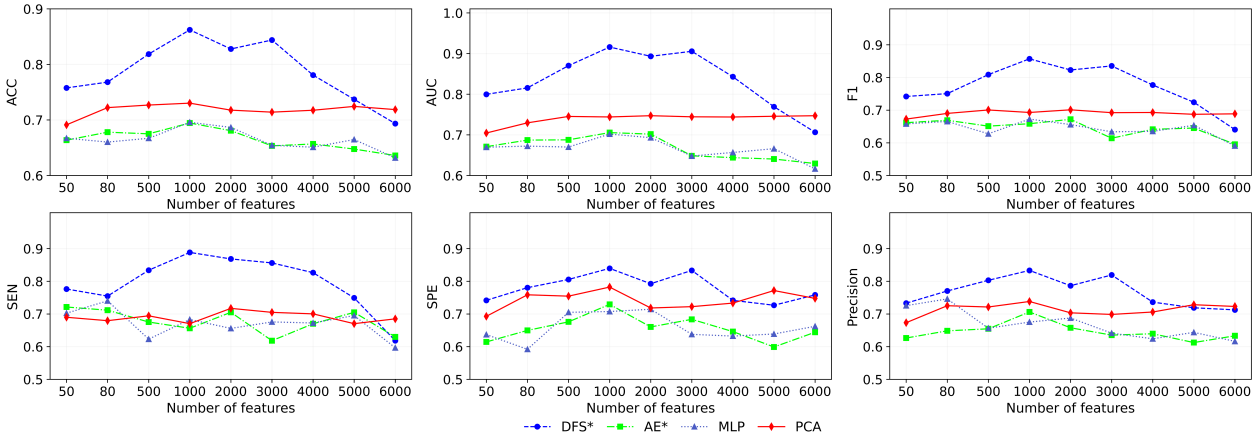


Fig. 2: Evaluation performance of the four methods with different numbers of features. For the PCA method, the corresponding feature counts are [50, 100, 200, 300, 400, 500, 600, 700, 800]. For example, the red solid line with diamond markers in the figure represents PCA, which achieves its highest ACC when the x-axis value reaches 1000. However, the optimal feature count for PCA should correspond to 300.

4 Discussion

4.1 The Most Discriminative Consensus Connection

Analyzing the brain regions involved in key functional connections is crucial for identifying essential neural links associated with the pathogenesis of ASD. This approach highlights the fundamental differences in brain connectivity between individuals with ASD and those with typical development (TD). To illustrate the relationship between the retained features and corresponding brain regions, we extracted the most discriminative consensus connections using a t-test and visualized them with the 'circularGraph' function (`https://github.com/paul-kassebaum-mathworks/circularGraph`). This was performed for thresholds of 0% and 50%, which correspond to fully connected brain networks and networks retaining only connections above the median threshold, respectively.

As shown in Fig. 4, 28 key consensus connections were identified from the fully connected network, while 29 connections were extracted at the 50% threshold. Both networks display

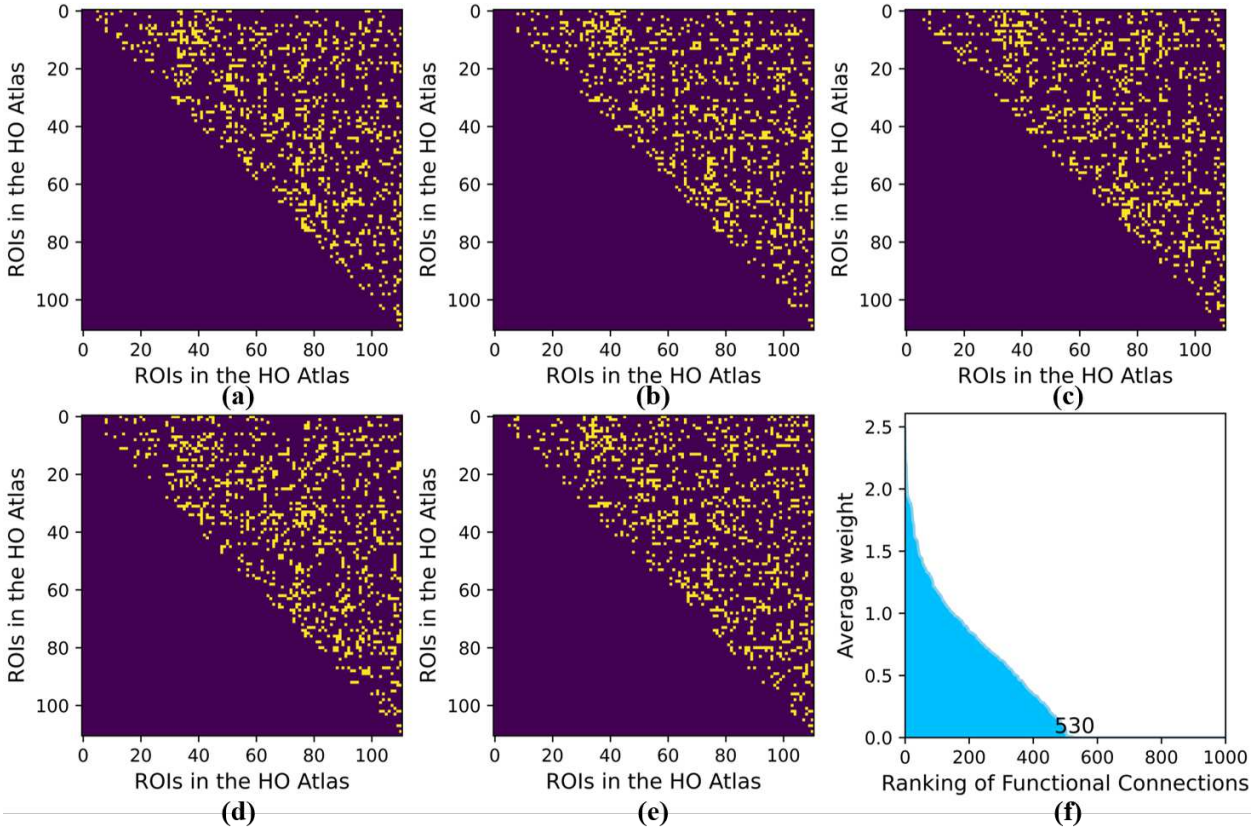


Fig. 3: The most important functional connections retained through five-fold cross-validation. (a) to (e) represent the features retained in each fold during the five-fold cross-validation process for the 111×111 matrix. The lower triangular part of the matrix and self-connections are excluded. Each row and column corresponds to one of the 111 brain regions defined by the HO atlas. If the connection value between region i and region j is 1 (indicated in yellow on the heatmap), the connection is retained; otherwise, it is set to 0 (indicated in purple on the heatmap). (f) illustrates the common features identified through the five-fold cross-validation process, ranked in descending order of importance.

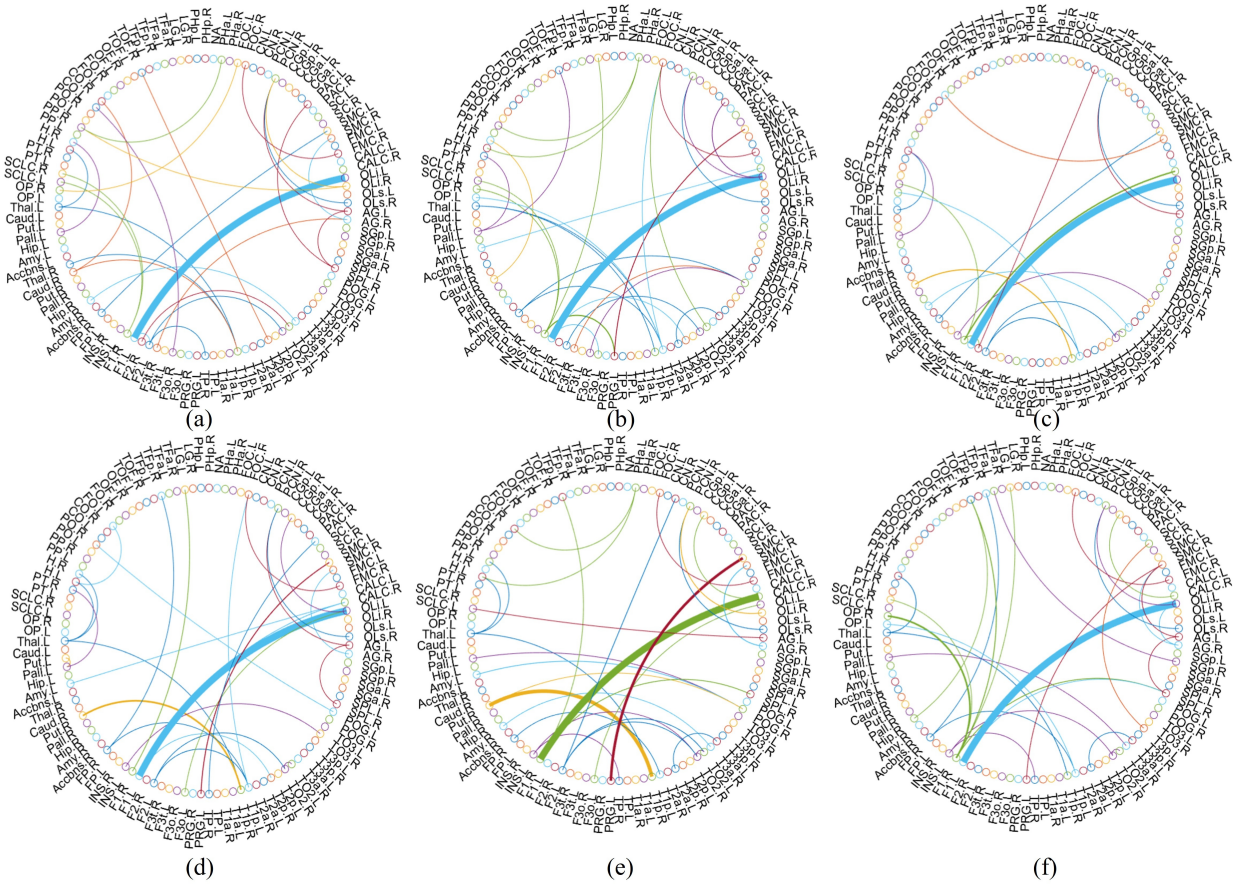


Fig. 4: Visualization of the most discriminative connectivity features (t-test, $p<0.01$). Arc colors are randomly assigned for distinction, and thickness reflects discriminative strength (inverse of p-value). Panels (a)–(f) show consensus connectivity maps from DFS using 0%, 10%, 20%, 30%, 40%, and 50% quantile thresholds.

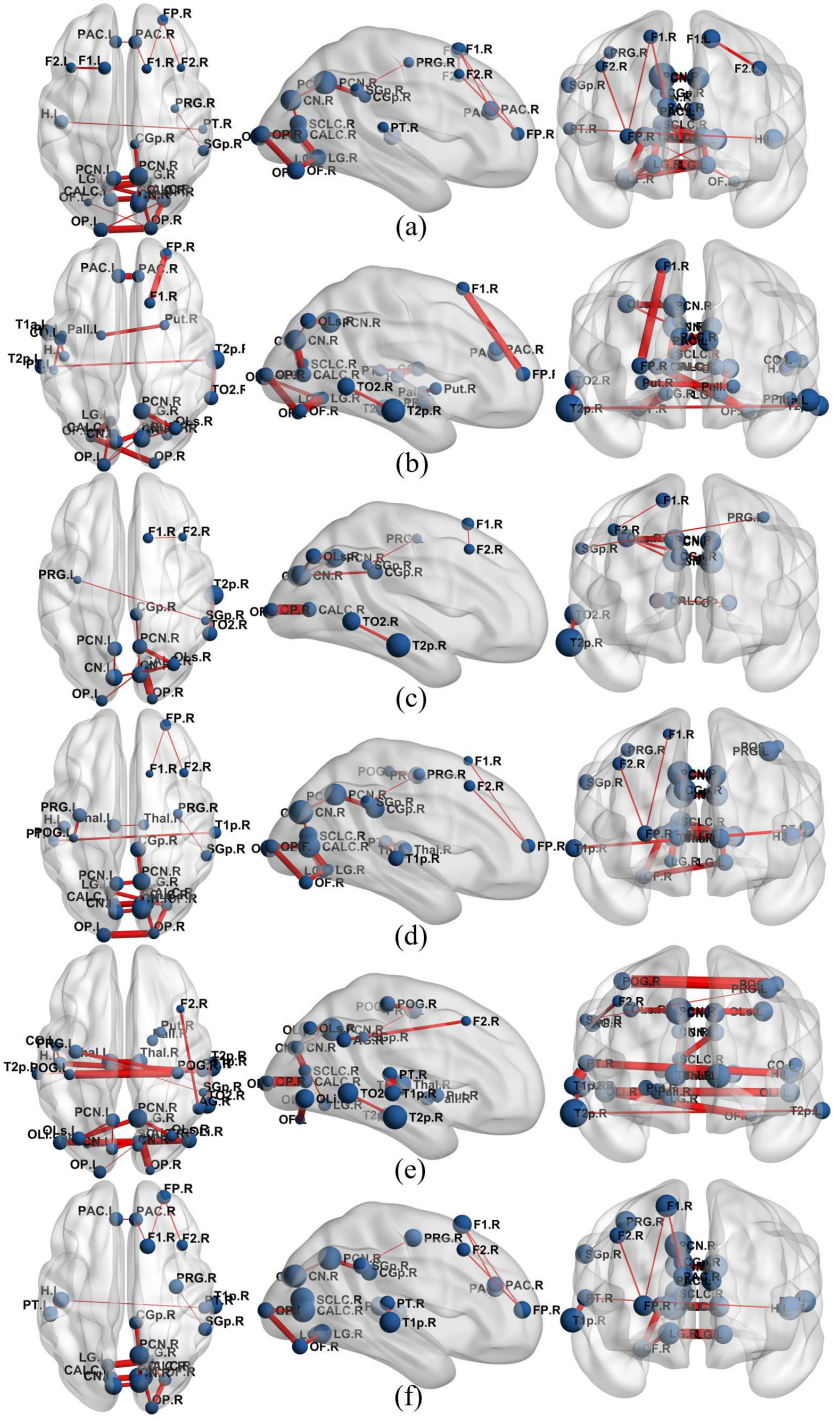


Fig. 5: Hub distribution of the top 10% functional connections in the ASD group. Node size indicates regional connectivity, and line thickness reflects connection strength. Panels (a)–(f) show 0%–50% quantile thresholds in axial, sagittal, and coronal views.

Table 4: Top 5 most discriminative connections selected from the ROIs in brain networks with different levels of sparsity (all p-values < 0.001).

Threshold	ROI A	ROI B	ASD	TD
0%	F1.L	OLi.L	0.39±0.20	0.36±0.22
0%	OLi.R	PCN.R	0.37±0.23	0.34±0.24
0%	F3t.R	AG.R	0.45±0.20	0.48±0.18
0%	Caud.R	T1p.R	0.11±0.22	0.10±0.22
0%	Thal.L	T1p.R	0.47±0.20	0.41±0.24
10%	OLi.R	PCN.R	0.37±0.05	0.34±0.06
10%	F3o.R	POG.R	0.28±0.05	0.25±0.05
10%	PRG.L	SMC.L	0.53±0.03	0.55±0.03
10%	OLi.L	PAC.L	0.23±0.04	0.21±0.05
10%	F1.R	OP.R	0.33±0.04	0.35±0.04
20%	F1.L	OLi.L	0.39±0.04	0.36±0.05
20%	F1.R	OP.R	0.33±0.05	0.35±0.04
20%	Put.R	T1p.R	0.47±0.03	0.42±0.05
20%	F2.L	T1p.L	0.29±0.05	0.31±0.05
20%	SMC.R	FO.L	0.37±0.04	0.37±0.05
Threshold	ROI A	ROI B	ASD	TD
30%	F1.L	OLi.L	0.39±0.21	0.35±0.23
30%	F1.L	CALC.R	0.29±0.23	0.33±0.22
30%	PRG.L	SMC.L	0.53±0.03	0.54±0.03
30%	Put.L	Pall.L	0.67±0.02	0.66±0.02
30%	F1.R	LG.L	0.23±0.05	0.26±0.05
40%	F1.L	OLi.L	0.38±0.05	0.34±0.06
40%	F1.R	CALC.R	0.26±0.05	0.30±0.05
40%	PRG.L	SMC.L	0.52±0.04	0.54±0.03
40%	AG.R	SMC.R	0.27±0.06	0.29±0.06
40%	OLi.R	PCN.R	0.35±0.06	0.30±0.07
50%	F1.R	CALC.R	0.24±0.06	0.28±0.06
50%	F1.L	OLi.L	0.36±0.06	0.32±0.06
50%	F1.R	TOF.R	0.16±0.24	0.20±0.24
50%	F1.R	SPL.R	0.23±0.26	0.22±0.27
50%	Thal.L	H.L	0.42±0.23	0.34±0.28

similar connection patterns, suggesting that the DFS method consistently selects comparable connections across brain networks with varying sparsity levels. We extracted the five most important connections at different sparsity levels (in Table 4) and found that the Superior Frontal Gyrus and Left Lateral Occipital Cortex (inferior division) exhibited the strongest discriminative power. The Superior Frontal Gyrus is linked to self-awareness and sensory coordination [40], and heightened functional connectivity in this region has been associated with social and communication challenges in children with autism [41, 42]. Additionally, the lateral occipital cortex is known to play a critical role in facial recognition in individuals with autism. Its increased volume and gyral enlargement may contribute to the visual processing abnormalities commonly observed in autistic individuals [43, 44]. Notably, alongside prominent regions like the Superior Frontal Gyrus and Left Lateral Occipital Cortex (inferior division), the Right Intracalcarine Cortex and Right Superior Temporal Gyrus (posterior division) also exhibit significant discriminative capabilities, particularly in nearly half of the sparse networks. Therefore, these regions warrant further investigation to better understand their potential roles in the neural mechanisms underlying autism.

4.2 Altered Pattern of the Brain Network Connectome

The top 10% of functional connections with the highest weights were identified as key hubs. As shown in Fig. 5, these ASD-related hubs are mainly located in the frontal, occipital, and parietal lobes. Notably, high-weight connections in the occipital lobe involve the occipital fusiform gyrus (OF), occipital pole (OP), intracalcarine cortex (CALC), and lingual gyrus (LG), which are critical for visual-spatial processing, body language, and emotion regulation [45]. Structural abnormalities in this region have been linked to IQ and ASD symptom severity [46, 47].

Both the frontal and parietal lobes show notable associations with ASD. The frontal lobe, involved in cognition, emotion, and motor control, is linked to motor and non-motor deficits in ASD [48]. The parietal lobe supports social communication and motor development, with reduced right-lobe connectivity associated with poorer praxis and social skills [49]. As shown in Fig. 5, the right hemisphere displays stronger connections than the left, particularly in the right frontal pole (FP.R), superior frontal gyrus (F1.R), and middle frontal gyrus (F2.R), reflecting functional asymmetries such as rightward bias in motor and insula networks and leftward bias in visual-spatial networks, which may underlie language-area shifts in ASD [50, 51].

4.3 Limitations

Several limitations should be considered. First, although ABIDE I is a large multisite dataset, evaluation was performed within the same aggregated cohort and did not include an independent external dataset. Second, differences in acquisition protocols, participant characteristics, and site composition may affect functional connectivity estimates and model performance. Third, the selected connections represent statistical associations and should not be interpreted as causal mechanisms or validated diagnostic biomarkers. Future studies should include site-held-out evaluation, harmonization analyses, and replication in independent cohorts such as ABIDE II.

5 Conclusion

This study presents a framework that combines deep feature selection with multi-sparsity functional connectivity networks to distinguish participants with autism from typically developing controls and to identify reproducible connectivity patterns. The strongest findings involved frontal, occipital, and parietal regions, including the superior frontal gyrus and lateral occipital cortex. These results support the value of examining connectivity across

multiple sparsity levels when studying autism-related brain network organization. Independent replication and external validation are required before the framework can be considered for clinical use.

Declarations

Funding

This work was supported by the Key Project of the Science and Technology Research Program of Chongqing Municipal Education Commission (Grant No. KJZD-K202600712), the Joint Training Base Construction Project for Graduate Students in Chongqing (Grant No. JDLHPYJD2021016), and the Key Laboratory of Complex Systems Optimization and Intelligent Control (Chongqing Municipal Education Commission) at Chongqing Jiaotong University.

Ethics approval and consent to participate

ABIDE I contains anonymized, previously collected data contributed by multiple sites. The original studies were conducted under site-specific institutional review board or ethics committee oversight, with informed consent or assent obtained according to local requirements. The present study involved secondary analysis of publicly available, de-identified data and included no new participant recruitment or intervention.

Consent for publication

Not applicable.

Data availability

The datasets analyzed during the current study are publicly available through the Autism Brain Imaging Data Exchange I (ABIDE I) repository at `https://www.nitrc.org/ir/data/projects/ABIDE`. Additional processed results supporting the findings are available from the corresponding author upon reasonable request.

Competing interests

The authors declare that they have no competing financial or non-financial interests related to this work.

Author contributions

L.Z. conceived and supervised the study, contributed to project administration, and reviewed and edited the manuscript. Y.D. contributed to the methodology, validation, and investigation, and reviewed and edited the manuscript. Z.Z. contributed to the methodology, software development, data curation, formal analysis, and visualization, and wrote the original draft of the manuscript. H.Z. contributed to validation and investigation and reviewed and edited the manuscript. L.H. provided resources, contributed to validation, and reviewed and edited the manuscript. All authors read and approved the final manuscript.

Acknowledgements

Not applicable.

Use of generative AI and AI-assisted technologies

During manuscript preparation, the authors used OpenAI ChatGPT for language editing and reformatting assistance. The authors reviewed, revised, and verified the resulting text and take full responsibility for the content of the manuscript. The tool was not used to perform data analysis or to alter the study results, interpretations, or conclusions.

References

[1] S. Rangasamy, S. R. D'mello, and V. Narayanan, "Epigenetics, autism spectrum, and neurodevelopmental disorders," *Neurotherapeutics*, vol. 10, no. 4, pp. 742–756, Oct. 2013, doi: 10.1007/s13311-013-0227-0.

[2] A. K. Sauer, J. E. Stanton, S. Hans, and A. M. Grabrucker, "Autism spectrum disorders: etiology and pathology," in *Autism Spectrum Disorders,* A. M. Grabrucker, Ed., AU: Exon Publications, 2021, [Online] Available: https://www.ncbi.nlm.nih.gov/books/NBK573613/.

[3] B. Ruggeri, U. Sarkans, G. Schumann, and A. M. Persico, "Biomarkers in autism spectrum disorder: the old and the new," *Psychopharmacology*, vol. 231, pp. 1201-1216, Mar. 2014, doi: 10.3390/life13071472.

[4] H. Zhuang et al., "Autism spectrum disorder: Pathogenesis, biomarker, and intervention therapy," *MedComm*, vol. 14, no. 3, pp. 319-351, Sept. 2012, doi: 10.1002/mco2.497.

[5] G. S. Dichter, "Functional magnetic resonance imaging of autism spectrum disorders," *Dialogues Clin. Neurosci.*, vol. 231, pp. 1201-1216, Mar. 2014, doi: 10.31887/DCNS.2012.14.3/gdichter.

[6] G. H. Glover, "Overview of functional magnetic resonance imaging," *Neurosurg. Clin. N. Am.*, vol. 22, no. 2, pp. 133-139, Apr. 2011, doi: 10.1016/j.nec.2010.11.001.

[7] C. Yen, C.-L. Lin, and M.-C. Chiang, "Exploring the frontiers of neuroimaging: a review of recent advances in understanding brain functioning and disorders," *Life*, vol. 13, no. 7, p. 1472, Jun. 2023, doi: 10.1007/s00213-013-3290-7.

[8] D. P. Kennedy and E. Courchesne, "The intrinsic functional organization of the brain is altered in autism," *NeuroImage*, vol. 39, no. 4, pp. 1877-1885, Feb. 2008, doi: 10.1016/j.neuroimage.2007.10.052.

[9] B. Biswal, F. Zerrin Yetkin, V. M. Haughton, and J. S. Hyde, "Functional connectivity in the motor cortex of resting human brain using echo-planar MRI," *Magn. Reson. Med.*, vol. 34, no. 4, pp. 537-541, Oct. 1995, doi: 10.1002/MRM.1910340409.

[10] C. S. Monk et al., "Abnormalities of intrinsic functional connectivity in autism spectrum disorders," *NeuroImage*, vol. 47, no. 2, pp. 764-772, Aug. 2009, doi: 10.1016/j.neuroimage.2009.04.069.

[11] A. Padmanabhan, C. J. Lynch, M. Schaer, and V. Menon, "The default mode network in autism," *Biol. Psychiatry Cogn. Neurosci. Neuroimaging*, vol. 2, no. 6, pp. 476-486, Sept. 2017, doi: 10.1016/j.bpsc.2017.04.004.

[12] C. J. Lynch et al., "Executive dysfunction in autism spectrum disorder is associated with a failure to modulate frontoparietal-insular hub architecture," *Biol. Psychiatry Cogn. Neurosci. Neuroimaging*, vol. 2, no. 6, pp. 537-545, Sept. 2017, doi: 10.1016/j.bpsc.2017.03.008.

[13] B. Chen et al., "BGreater functional connectivity between sensory networks is related to symptom severity in toddlers with autism spectrum disorder," *J. Child Psychol. Psychiatry*, vol. 62, no. 2, pp. 160-170, May. 2021, doi: 10.1111/jcpp.13268.

[14] R. A. Bahathiq, H. Banjar, A. K. Bamaga, and S. K. Jarraya, "Machine learning for autism spectrum disorder diagnosis using structural magnetic resonance imaging: Promising but challenging," *Front. Neuroinform.*, vol. 16, p. 949926, Sept. 2022, doi: 10.3389/fninf.2022.949926.

[15] M. Quaak, L. van de Mortel, R. M. Thomas, and G. van Wingen, "Deep learning applications for the classification of psychiatric disorders using neuroimaging data: systematic review and meta-analysis," *Neuroimage Clin.*, vol. 30, p. 102584, Jun. 2021, doi: 10.1016/j.nicl.2021.102584.

[16] J. Hu, L. Cao, T. Li, B. Liao, S. Dong, and P. Li, "Interpretable Learning Approaches in Resting-state Functional Connectivity Analysis: The Case of Autism Spectrum Disorder," *Comput. Math. Methods. Med.*, vol. 2020, no. 1, p. 1394830, May. 2020, doi: 10.1155/2020/1394830.

[17] Z. Rakhimberdina, X. Liu, and T. Murata, "Population graph-based multi-model ensemble method for diagnosing autism spectrum disorder," *Sensors*, vol. 20, no. 21, p. 6001, Oct. 2020, doi: 10.3390/s20216001.

[18] L. Shao, C. Fu, and X. Chen, "A heterogeneous graph convolutional attention network method for classification of autism spectrum disorder," *BMC Bioinform.*, vol. 24, no. 1, p. 363, Sept. 2023, doi: 10.1186/s12859-023-05495-7.

[19] Y. Li, C.-Y. Chen, and W. W. Wasserman, "Deep feature selection: theory and application to identify enhancers and promoters," *J. Comput. Biol.*, vol. 23, no. 5, pp. 322-336, Apr. 2016, doi: 10.1007/978-3-319-16706-0_20.

[20] L. Shao, C. Fu, Y. You, and D. Fu, "Classification of ASD based on fMRI data with deep learning," *Cogn. Neurodyn.*, vol. 15, no. 6, pp. 961-974, May. 2021, doi: 10.1007/s11571-021-09683-0.

[21] Y. Chen, Q. Gao, F. Liang, and X. Wang, "Nonlinear variable selection via deep neural networks," *J. Comput. Graph. Stat.*, vol. 30, no. 2, pp. 484-492, Oct. 2021, doi: 10.1080/10618600.2020.1814305.

[22] Z. Lai and H. Deng, "Medical image classification based on deep features extracted by deep model and statistic feature fusion with multilayer perceptron," *Comput. Intell. Neurosci.*, vol. 2018, no. 1, pp. 2061516, Sept. 2018, doi: 10.1155/2018/2061516.

[23] A. Abraham et al., "Deriving reproducible biomarkers from multi-site resting-state data: An Autism-based example," *NeuroImage*, vol. 147, pp. 736-745, Nov. 2017, doi: 10.1016/j.neuroimage.2016.10.045.

[24] S. Parisot et al., "Disease prediction using graph convolutional networks: application to autism spectrum disorder and Alzheimer's disease," *Med. Image Anal.*, vol. 48, pp. 117-130, Jun. 2018, doi: 10.1016/j.media.2018.06.001.

[25] C. Craddock et al., "The neuro bureau preprocessing initiative: open sharing of preprocessed neuroimaging data and derivatives," *Front. Neuroinform.*, vol. 7, no. 27, p. 5, 2013, doi: 10.3389/CONF.FNINF.2013.09.00041.

[26] N. U. Dosenbach et al., "Prediction of individual brain maturity using fMRI," *Science*, vol. 329, no. 5997, pp. 1358-1361, Sept. 2010, doi: 10.1126/science.1194144.

[27] R. C. Craddock, G. A. James, P. E. Holtzheimer III, X. P. Hu, and H. S. Mayberg, "A whole brain fMRI atlas generated via spatially constrained spectral clustering," *Hum. Brain Mapp.*, vol. 33, no. 8, pp. 1914-1928, Aug. 2012, doi: doi: 10.1002/hbm.21333.

[28] N. Makris et al., "Decreased volume of left and total anterior insular lobule in schizophrenia," *Schizophr. Res.*, vol. 83, no. 2-3, pp. 155-171, Apr. 2006, doi: 10.1016/j.schres.2005.11.020.

[29] R. S. Desikan et al., "An automated labeling system for subdividing the human cerebral cortex on MRI scans into gyral based regions of interest," *NeuroImage*, vol. 31, no. 3, pp. 968-980, Jul. 2006, doi: 10.1016/j.neuroimage.2006.01.021..

[30] J. A. Frazier et al., "Structural brain magnetic resonance imaging of limbic and thalamic volumes in pediatric bipolar disorder," *Am. J. Psychiatry*, vol. 162, no. 7, pp. 1256-1265, Jul. 2005, doi: 10.1176/APPI.AJP.162.7.1256.

[31] J. M. Goldstein et al., "Hypothalamic abnormalities in schizophrenia: sex effects and genetic vulnerability," *Biol. Psychiatry*, vol. 61, no. 8, pp. 935-945, Apr. 2007, doi: 10.1016/j.biopsych.2006.06.027.

[32] W. Li, L. Zhang, L. Qiao, and D. Shen, "Toward a better estimation of functional brain network for mild cognitive impairment identification: a transfer learning view," *IEEE J. Biomed. Heal. Inf.*, vol. 24, no. 4, pp. 1160-1168, Jun. 2019, doi: 10.1109/JBHI.2019.2934230.

[33] W. Li, X. Xu, Z. Wang, L. Peng, P. Wang, and X. Gao, "Multiple connection pattern combination from single-mode data for mild cognitive impairment identification," *Front. Cell Dev. Biol.*, vol. 9, p. 782727, Nov. 2021, doi: 10.3389/fcell.2021.782727.

[34] W.-K. Li, Y.-C. Chen, X.-W. Xu, X. Wang, and X. Gao, "Human-guided functional connectivity network estimation for chronic tinnitus identification: a modularity view," *IEEE J. Biomed. Heal. Inf.*, vol. 26, no. 10, pp. 4849-4858, Jul. 2022, doi: 10.1109/JBHI.2022.3190277.

[35] C. M. Bishop and N. M. Nasrabadi, "Linear Models for Classification," in *Pattern recognition and machine learning,*4th ed., vol. 4, M. Jordan, Ed. New York, NY, USA: springer, 2006, pp.162-164.

[36] J. Liu, Y. Sheng, W. Lan, R. Guo, Y. Wang, and J. Wang, "Improved ASD classification using dynamic functional connectivity and multi-task feature selection," *Pattern Recognit. Lett.*, vol. 138, pp. 82-87, Oct. 2020, doi: 10.1016/j.patrec.2020.07.005.

[37] G. Wen, P. Cao, H. Bao, W. Yang, T. Zheng, and O. Zaiane, "MVS-GCN: A prior brain structure learning-guided multi-view graph convolution network for autism spectrum disorder diagnosis," *Comput. Biol. Med.*, vol. 142, p. 105239, Jan. 2022, doi: 10.1016/j.compbiomed.2022.105239.

[38] W. Yin, S. Mostafa, and F.-X. Wu, "Diagnosis of autism spectrum disorder based on functional brain networks with deep learning," *J. Comput. Biol.*, vol. 28, no. 2, pp. 146-165, Oct. 2021, doi: 10.1089/cmb.2020.0252.

[39] M. Wang, J. Guo, Y. Wang, M. Yu, and J. Guo, "Multimodal autism spectrum disorder diagnosis method based on DeepGCN," *IEEE Trans. Neural Syst. Rehabilitation Eng.*, vol. 31, pp. 3664-3674, Sept. 2023, doi: 10.1109/TNSRE.2023.3314516.

[40] I. I. Goldberg, M. Harel, and R. Malach, "When the brain loses its self: prefrontal inactivation during sensorimotor processing," *Neuron*, vol. 50, no. 2, pp. 329-339, Apr. 2006, doi: 10.1016/j.neuron.2006.03.015.

[41] S. Xu et al., "Altered functional connectivity in children with low-function autism spectrum disorders," *Front. Neurosci.*, vol. 13, p. 806, Aug. 2019, doi: 10.3389/fnins.2019.00806.

[42] M. Assaf et al., "Abnormal functional connectivity of default mode sub-networks in autism spectrum disorder patients," *NeuroImage*, vol. 53, no. 1, pp. 247-256, Oct. 2010, doi: 10.1016/j.neuroimage.2010.05.067.

[43] C. Ecker, S. Y. Bookheimer, and D. G. Murphy, "Neuroimaging in autism spectrum disorder: brain structure and function across the lifespan," *Lancet Neurol.*, vol. 14, no. 11, pp. 1121-1134, Nov. 2015, doi: 10.1016/S1474-4422(15)00050-2.

[44] B. Keehn, L. Brenner, E. Palmer, A. J. Lincoln, and R.-A. Mueller, "Functional brain organization for visual search in ASD," *J. Int. Neuropsychol. Soc.*, vol. 14, no. 6, pp. 990-1003, Oct. 2008, doi: 10.1017/S1355617708081356.

[45] L. E. Libero, C. E. Stevens Jr, and R. K. Kana, "Attribution of emotions to body postures: An independent component analysis study of functional connectivity in autism," *Hum. Brain Mapp.*, vol. 35, no. 10, pp. 5204-5218, Oct. 2014, doi: 10.1002/hbm.22544.

[46] T. Nickl-Jockschat et al., "Brain structure anomalies in autism spectrum disorder–a meta-analysis of VBM studies using anatomic likelihood estimation," *Hum. Brain Mapp.*, vol. 33, no. 6, pp. 1470-1489, Jun. 2012, doi: 10.1002/hbm.21299.

[47] H. Wang et al., "Developmental brain structural atypicalities in autism: a voxel-based morphometry analysis," *Child Adolesc. Psychiatry Ment. Health*, vol. 16, no. 1, p. 7, Nov. 2022, doi: 10.1186/s13034-022-00443-4.

[48] G. Leisman, R. Melillo, and T. Melillo, "Prefrontal functional connectivities in autism spectrum disorders: A connectopathic disorder affecting movement, interoception, and cognition," *Brain Res. Bull.*, vol. 198, pp. 65-76, Apr. 2023, doi: 10.1016/j.brainresbull.2023.04.004.

[49] N. F. Wymbs, M. B. Nebel, J. B. Ewen, and S. H. Mostofsky, "Altered inferior parietal functional connectivity is correlated with praxis and social skill performance in children with autism spectrum disorder," *Cereb. Cortex*, vol. 31, no. 5, pp. 2639-2652, Dec. 2021, doi: 10.1093/cercor/bhaa380.

[50] D. L. Floris et al., "Atypical brain asymmetry in autism–a candidate for clinically meaningful stratification," *Biol. Psychiatry Cogn. Neurosci. Neuroimaging*, vol. 6, no. 8, pp. 802-812, Mar. 2021, doi: 10.1101/2020.03.24.000349.

[51] M. R. Herbert et al., "Brain asymmetries in autism and developmental language disorder: a nested whole-brain analysis," *Brain*, vol. 128, no. 1, pp. 213-226, Nov. 2005, doi: 10.1093/BRAIN/AWH330.